Recent TCV Results – Innovative Plasma Shaping to Improve Plasma Properties and Insight*)

Antoine POCHELON, Paolo ANGELINO, Roland BEHN, Stephan BRUNNER, Stefano CODA, Nataliya KIRNEVA[1)], Sergei Yu MEDVEDEV[2)], Holger REIMERDES, Jonathan ROSSEL, Olivier SAUTER, Laurent VILLARD, Dávid WÁGNER, Alberto BOTTINO[3)], Yann CAMENEN[4)], Gustavo P. CANAL, Prabal K. CHATTOPADHYAY[5)], Basil P. DUVAL, Ambrogio FASOLI, Timothy P. GOODMAN, Sébastien JOLLIET, Alexander KARPUSHOV, Benoît LABIT, Alessandro MARINONI, Jean-Marc MORET, Andreas PITZSCHKE, Laurie PORTE, Mikael RANCIC, Victor S. UDINTSEV[6)] and the TCV Team

Ecole Polytechnique Fédérale de Lausanne (EPFL), Centre de Recherches en Physique des Plasmas, Association Euratom-Confédération Suisse, CH-1015 Lausanne, Switzerland
[1)]*NRC-Kurchatov Institute, Kurchatov Sq. 1, 123182 Moscow, Russia*
[2)]*Keldysh Institute, Russian Academy of Sciences, Miusskaya Sq. 4, 125047 Moscow, Russia*
[3)]*Max-Planck Institut für Plasmaphysik, IPP-Euratom Association, Garching bei München, Germany*
[4)]*PIIM UMR7345, CNRS/Aix-Marseille University, France*
[5)]*Institut for Plasma Physics, Bhat, Gandhinagar, Gujarat, India*
[6)]*ITER Organisation, St Paul lez Durance, France*

(Received 15 January 2012 / Accepted 10 August 2012)

The TCV tokamak facility is used to study the effect of innovative plasma shapes on core and edge confinement properties. In low collisionality L-mode plasmas with electron cyclotron heating (ECH) confinement increases with increasing negative triangularity δ. The confinement improvement correlates with a decrease of the inner core electron heat transport, even though triangularity vanishes to the core, pointing to the effect of non-local transport properties. TCV has recently started the study of the effects of negative triangularity in H-mode plasmas. H-mode confinement is known to improve towards positive triangularity, due to the increase of pedestal height, though plagued by increasingly large edge localised modes (ELMs). An optimum triangularity could thus be sought between steep edge barriers ($\delta > 0$) with large ELMs, and improved core confinement ($\delta < 0$) with small ELMs. This opens the possibility for a reactor of having H-mode-level confinement within an L-mode edge, or at least with mitigated ELMs. In TCV, ELMy H-modes with upper triangularity $\delta_{\mathrm{top}} < 0$ are explored, showing a reduction of ELM peak energy losses compared to $\delta_{\mathrm{top}} > 0$. Alternative shapes are proposed on the basis of ideal MHD stability calculations. Shaping has the potential to bring at the same time key solutions to confinement, stability and wall loading issues and, from the comparison of experimental and simulation results, to give deeper insight in transport and stability.

Keywords: confinement, plasma shape, triangularity, global transport, gyrokinetic simulation, H-mode, ELM

DOI: 10.1585/pfr.7.2502148

1. Introduction

Transport and stability are central issues of magnetic fusion, since high energy confinement time and plasma pressure are key ingredients for an economical reactor. In a tokamak reactor, instabilities relaxing power pulses can lead to severe or non-tolerable erosion of the first wall. Plasma shaping, by influencing both confinement and stability properties [1], can be used as a free parameter in the optimization of the design of a reactor, in parallel with ITER.

Apart from enhancing performance, there are other solid motivations justifying to study plasma shapes other than those possible in ITER. Shaping is an excellent tool for the test and validation of plasma modelling, in particular for transport and stability. The usual confinement scaling laws exhibit no triangularity dependence, but confinement in TCV plasma core improves towards negative triangularity ($\delta < 0$) in low collisional L-mode discharges when in the trapped electron mode (TEM) turbulence regime – a regime likely to occur in reactor conditions. In contrast, it is well established from different tokamak H-mode studies that both the pedestal heights and ELM sizes increase as δ increases, and thus confinement increases with triangu-

author's e-mail: Antoine.Pochelon@epfl.ch
*) This article is based on the invited presentation at the 21st International Toki Conference (ITC21).

larity in the positive triangularity domain. It is therefore of great interest to explore the properties of H-modes at negative δ, which so far have not been explored.

Our long-term goal is to optimize plasma operation by changing plasma triangularity, including in the negative triangularity range, to maximize core confinement and mitigate ELMs.

The paper is constructed as follows. The introduction describes different effects of plasma shape on confinement and stability, focusing on triangularity. The improved confinement and transport properties obtained at negative triangularity in low collisionality TEM are summarized in section 2 and compared with local and global gyrokinetic modelling in section 3. The exploration of the new domain of H-mode at negative triangularity is the subject of section 4, followed in section 5 by the MHD stability analysis relevant to the H-mode experiments developed, and prospects gained from these calculations.

This paper describes the first systematic study of negative triangularity H-modes. To develop reliable H-mode operation, it was important to use equilibria that could efficiently be heated in H-mode with the presently available additional heating system setup in TCV. This resulted – as a first step - in a choice of equilibria in the H-mode section 4 that are so far different from the ones in the confinement sections 2-3. In brief, the low collisionality strongly benefiting negative triangularity confinement is difficult to reach in TCV H-mode, because the H-mode can only be maintained at higher densities.

2. Confinement and Transport Improvement with Negative Triangularity ($\delta < 0$)

The TCV tokamak [2] ($R = 0.88$ m, $a = 0.25$ m, $R/a \sim 3.5$, $B \leq 1.5$ T, $I_p \leq 1$ MA) offers extreme shaping flexibility with its 16 independent poloidal field coils, which allowed us to achieve: elongation $0.9 < \kappa < 2.8$, triangularity $-0.7 < \delta < 1$, varied squareness, single null (SN), double null (DN), and snowflake divertor. This flexibility in shape is matched by a flexible ECH system [3]: 4.5 MW at 2nd (X2) and 3rd (X3) harmonic with 7 independent launchers enabling local power deposition for any plasma shape.

Energy confinement was found to improve towards $\delta < 0$ in low-density EC heated L-mode plasmas, (Fig. 1) [4, 5], a surprising result in contrast to earlier results in medium density Ohmic plasmas, where a weaker effect of triangularity was observed [6]. The ECH plasma conditions in which a definite effect was found are: low-density ECH plasmas, high normalized electron temperature gradient $R/L_{Te} > 7$ and $T_e/T_i \sim$ 3-5, that is in the TEM dominated regime and in the low collisionality domain, $\nu_{eff} \sim$ 0.2-1, later identified as being a crucial parameter [7] (where $\nu_{eff} \approx 0.1 R Z_{eff} n_e/T_e$, with lengths in m, densities in 10^{19} m^{-3} and temperatures in keV, see [8]).

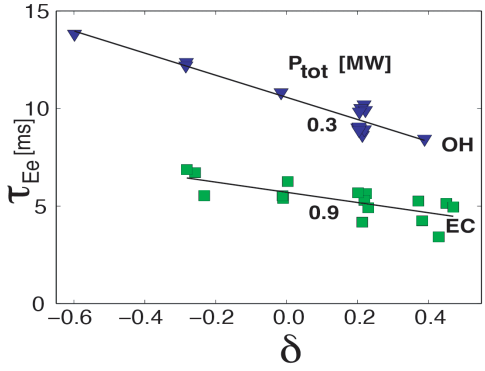

Fig. 1 Confinement time as a function of triangularity for two different powers, 0.3 and 0.9 MW, in low collisionality plasmas [5].

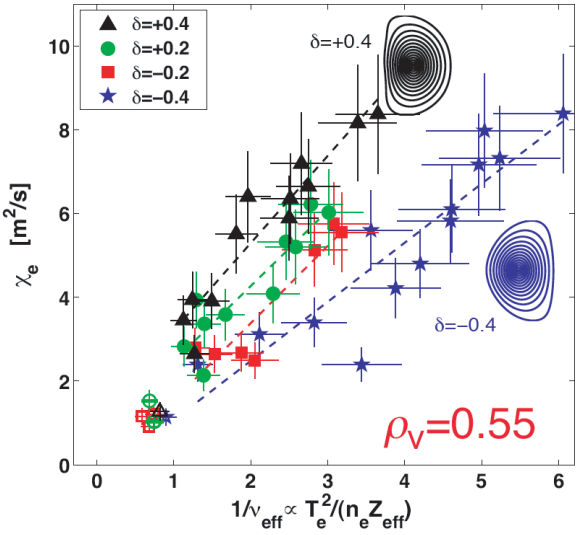

Fig. 2 Heat flux diffusivity measured at mid-radius for a scan of positive and negative triangularities versus inverse collisionality, χ_e versus $(1/\nu_{eff})$ [9].

Local heat deposition with ECH enabled exhaustive local heat transport measurements at mid-radius, over a wide range of T_e and R/L_{Te}, which allowed isolating collisionality ν_{eff} as a key element. The heat diffusivity χ_e increases with triangularity and decreases with ν_{eff}; the heat diffusivity is typically reduced by a factor 2 from $\delta = 0.4$ to -0.4 over a wide range of collisionality $\nu_{eff} < 1$ (Fig. 2) [9]. This means also that sustaining at negative triangularity $\delta = -0.4$ a pressure profile identical to the one at $\delta = 0.4$ requires only half the power [9]. It follows from the same experiments that χ_e is halved *over all radii* outside the heat deposition location, here located just outside the $q = 1$ radius at $\rho_v \sim 0.3$ (see e.g. Fig. 6 in [10]). The collisionality value at which the effects of triangularity start to vanish is typically $\nu_{eff} \sim 1$ in Fig. 2, and at higher collisionality values in the range $\nu_{eff} \sim$ 2.5-10, as in the higher-density Ohmic experiments of [6], only a weak, residual effect of triangularity was seen.

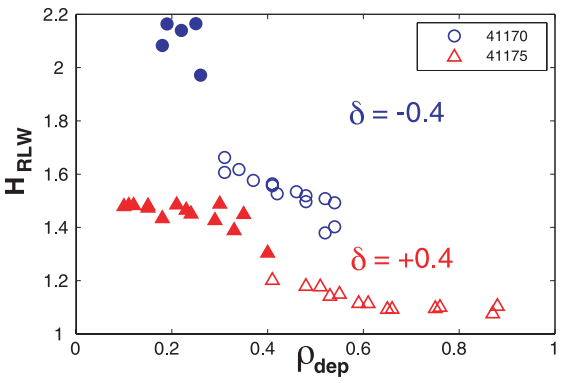

Fig. 3 Dependence of the confinement factor H_{RLW} in a sweep of radial EC-power deposition for a negative and a positive triangularity δ discharge, showing improved confinement at negative δ at all deposition radii, including at the very core. Open symbols: deposition outside the $q = 1$ region, and solid, inside [11].

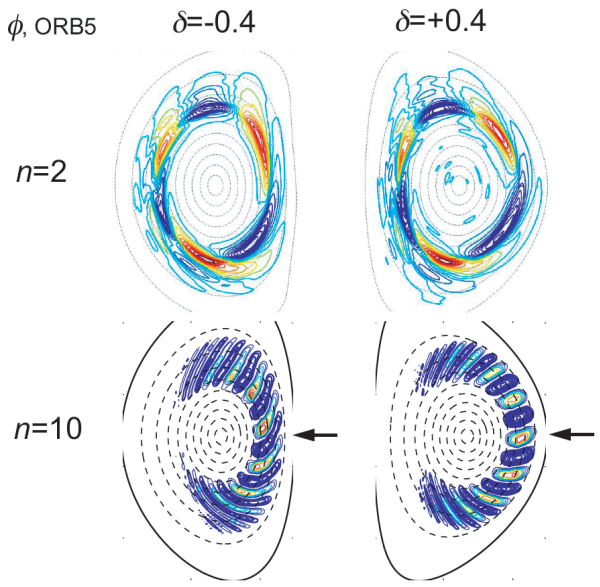

Fig. 4 Poloidal plot of the potential for transport relevant low n TEM showing large radial extension and visible reduction (arrow) in the perpendicular wavelength for $n = 2$, 10.

An alternative way of demonstrating the effect of triangularity on transport deep inside the plasma is to measure the confinement response to a radial sweep of constant power deposition. This is shown in Fig. 3, where the improvement factor over the standard L-mode, H_{RLW}, is shown as a function of the radius of power deposition [11]. The resulting confinement is best for power deposition close to plasma axis, particularly inside $q = 1$, and decreases as the deposition moves to the edge, as known. The H-factor is substantially higher at negative triangularity ($\delta = -0.4$) compared to positive ($\delta = +0.4$), and the beneficial effect on confinement extends deep in the core, even though the "geometric" triangularity, decays quickly from the edge (δ at mid-radius is 25% of the edge value). This is a possible indication of the presence of global effects in TEM induced transport.

3. Comparison with Transport Models – Global Transport Effects

In this section, we study the effect of plasma triangularity by comparing linear and nonlinear (local) transport models and local and global (linear) transport models. This approach should allow determining the most relevant and efficient model needed for the cross-validation of experiment and theory in the present shape variation experiments.

3.1 Local GK simulations

Local (flux-tube) gyrokinetic simulations with the GS2 [12] code indicate that most of the TEM transport, as estimated from quasilinear theory, occurs in the range $k_\theta \rho_i \sim 0.3$, which is also the range mostly affected by triangularity changes [10]. The local quasilinear estimate of the heat diffusivity decreases towards $\delta < 0$ [10], showing already the same trend as in the experiment. Note that all the simulations are based on actual TCV ideal MHD equilibria.

The local heat flux diffusivity χ_e can also be obtained with GS2 runs in nonlinear mode at different radial depths [10]. The ratio $\chi_e(\delta = +0.4)/\chi_e(\delta = -0.4)$ and its radial dependence are a measure of the change of transport with triangularity and of the penetration of triangularity effects. The triangularity effect on χ_e is found to vanish rapidly towards the centre of the plasma in this local gyrokinetic calculation, in fact as rapidly as the local geometric triangularity decreases towards the centre. This stands in contrast to the experimental χ_e from power balance, for which the triangularity effect on χ_e penetrates to the plasma core.

The non-linear flux-tube – local – GS2 calculations predict correctly the trend of χ_e to decrease with increasing collisionality ν_{eff}, when trying to reproduce the experimental behaviour shown in (Fig. 2). But these simulations can only predict a correct difference due to triangularity in the plasma periphery and at the lowest collisionalities, in marked contrast to the effect seen in the experiment.

These difficulties suggest that there might be a stronger radial link mediating transport between core and edge, which can only be addressed within the frame of a global approach.

3.2 Global GK simulations

Global transport effects are expected for finite but not too small values of $\rho^* \equiv \rho_L/a$. In TCV, $\rho^* \sim 1/70$, thus finite ρ^* effects may be important, giving rise to differences between local and global simulations. Here, the global gyrokinetic code ORB5 [13] enables us to carry out linear and nonlinear simulations. In this paper, to evaluate the effect of triangularity on transport, linear runs have been carried out using actual TCV ideal MHD equilibria [7].

Triangularity shaping does have an effect on the global linear mode structure. Figure 4 shows contour plots of the perturbed potential in the poloidal cross-section of negative ($\delta = -0.4$) and positive ($\delta = +0.4$) triangularity ideal MHD equilibria. The most noticeable effect of negative triangularity shaping is the distortion of the radial structures of intermediate mode numbers, resulting in an increase in k_r at the equatorial low field side midplane, arrows in (Fig. 4). In the case of $n = 10$, the tilt of the potential cells is very different for the two triangularities, leading to a factor two different k_r, that is a factor two smaller radial wavelength for the negative triangularity case. Further works involving nonlinear global gyrokinetic simulations should be performed in order to find out whether the effect observed on the linear mode structures has an effect on the turbulent transport level. Moreover, it should be noted that changing the edge triangularity also changes the Shafranov shift. More work is thus required to discriminate the intrinsic effects of triangularity and Shafranov shift. Note also that in TEM cases the nonlinear saturation mechanism seems to be less dependent on the interaction with zonal flows than in typical ITG dominated case [14].

4. H-mode Properties at Negative Triangularity – ELM Mitigation

4.1 ELM behaviour

One would like to know whether the beneficial effects of negative triangularity found in L-mode could be extended to H-mode. However, H-mode at negative triangularity is yet totally unexplored.

Reliable H-mode operation at negative triangularity was developed recently in teardrop-shaped, centred single null (SNC) discharges. This plasma configuration, with the X-point located on the 2nd harmonic electron cyclotron resonance (X2), provides optimal access to the EC resonance for efficient edge plasma heating, even in plasmas that are slightly overdense in the centre (Fig. 5 left). Robust, 99% first pass X2 absorption inside the separatrix, with power typically 1.5-2.5 times above H-mode threshold, enables control over the ELM type regime. The X2 power, 300-900 kW, is deposited at a location close to the edge, $\rho_{dep} = 0.9$, unchanged during the triangularity sweep (Fig. 5 right). The X3 power is launched from the top with a poloidal angle that maximizes absorption during the shape change. Typically, 500-700 kW of X3 power are absorbed close to the core. Different EC power waveforms have been explored. In these experiments, the main plasma parameters are: elongation $\kappa = 1.7$, upper triangularity δ_{top} = +0.2 to −0.2 (with $\delta_{top} \equiv -(R_{top\,max} - R_{axis})/a$, where $R_{top\,max}$ is the major radius of maximum height of the last closed flux surface, a is the plasma radius at equator), $q_{95} = 2.3$, n_{eav} ~3.5 10^{19} m^{-3}, $B \times \nabla B$ towards X-point. The triangularity dependence of H-mode properties and ELM behaviour has been studied by continuously varying the upper triangularity in the range $-0.2 < \delta_{top} < +0.2$ during one discharge, as indicated in (Fig. 5).

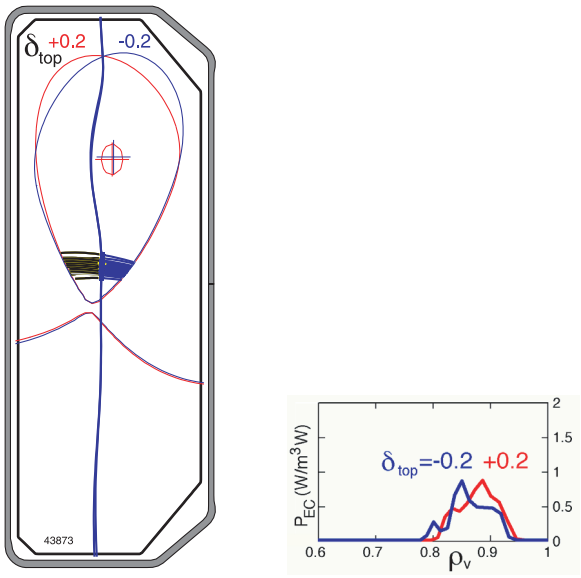

Fig. 5 Left: Single Null Centred (SNC) equilibrium, with triangularity swept from $\delta_{top} = +0.2$ to −0.2, together with the X2 heating beam path used to control the H-mode regime. The cold resonance crossing the X-point provides good X2 access. Right: X2 power deposition location maintained constant throughout shape sweep.

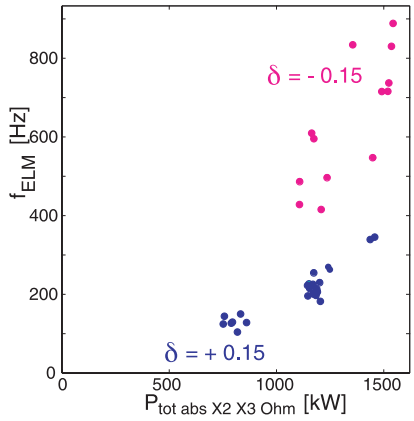

Fig. 6 Power dependence of ELM frequency: f_{ELM} increases with power for both positive and negative triangularity, indicating type I ELM regime all over the triangularity domain. Negative triangularity leads to higher frequency ELMs.

For both positive and negative triangularity, the ELM frequency f_{ELM} increases with increasing total power (P_{tot} = P_{X2} + P_{X3} + P_{OH}), which identifies the ELMs as type I, as shown in Fig. 6.

The ELM amplitude is found to decrease towards $\delta < 0$, as seen from the D_α emission and the diamagnetic loop [15], yielding the relative energy loss $\Delta W_{ELM}/W$, while the ELM frequency is found to increase. Over the range δ_{top} = +0.2 to −0.2, negative triangularity brings a three-fold increase in f_{ELM} and a three-fold reduction of peak losses,

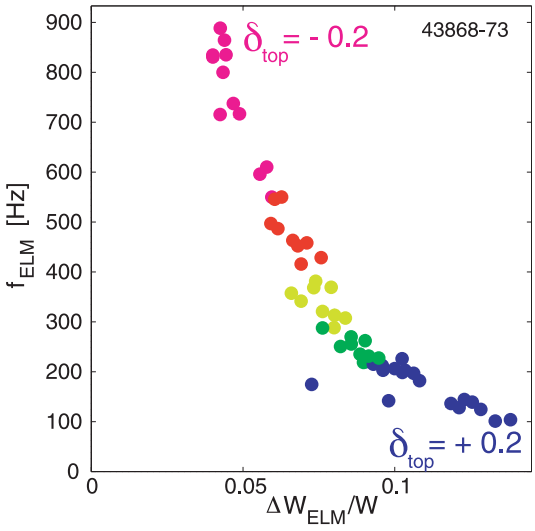

Fig. 7 Type I ELM amplitude and frequency for different triangularities δ_{top}. Towards negative triangularity, the ELM frequency increases and the relative ELM energy loss decreases, both by a factor of 3 over the range δ_{top} = +0.2 to −0.2. The colour scale represents 5 equal size classes of triangularities.

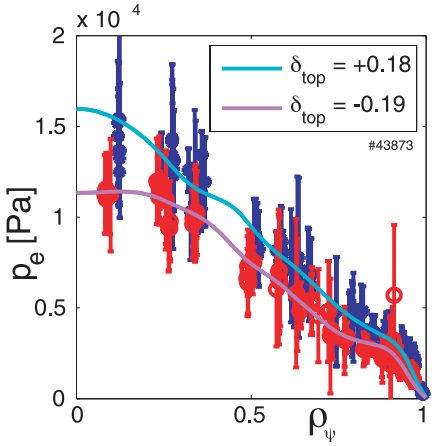

Fig. 8 Electron pressure profiles for positive and negative triangularity (δ_{top} = ±0.2), time-averaged (including the ELM events), showing the reduction in pedestal height towards negative triangularity.

$\Delta W_{ELM}/W$, as shown in Fig. 7.

Throughout the triangularity scan, care was taken to fix the location of X2 power deposition. This is important, as it was observed recently that f_{ELM} increases with the deposition location moving to the edge [16] in similar discharges. In the current δ_{top}-scan, the X2 power deposition location was maintained roughly constant at $\rho_{dep} = 0.9$ (ρ_v-units). The displacement is less than 1%, which cannot explain the ELM frequency variation.

4.2 Confinement analysis in H-mode

After having decreased the ELM energy loss by reducing triangularity towards negative values, one would wish to determine the specific contributions of core transport and edge barrier to the confinement as a function of triangularity. Due to overdense central density, the predominant edge-heating scheme is well suited for the control of the ELM regime, however less optimal for aiming at confinement studies.

The electron pressure profiles from Thomson scattering at $\delta_{top} = \pm 0.2$ are shown in Fig. 8. Between δ_{top} = +0.2 and −0.2, the p_e pedestal height decreases by ~20%. Thus, the increase of pedestal height with δ, well identified in the $\delta > 0$ range [17], extends further to negative triangularity. In addition, both profiles have similar R/L_{pe} in the core.

A preliminary analysis of the confinement regime yields: collisionality ν_{eff} ~1 measured at $\rho_v \sim 0.5$, R/L_n = 2-3, R/L_{T_e} = 10 but low R/L_{T_i}. The GS2 transport code indicates TEM dominated regime for both triangularities δ_{top} = ±0.2. The densities, or more crucially the collisionalities, are higher than in the earlier L-mode experiments that showed an improved confinement at $\delta < 0$ [9].

The total energy confinement time τ_E normalized to TCV scaling ($\tau_E/n_e^{0.46}P^{-0.7}$) [4] shows a similar 30% decrease towards $\delta < 0$, similar to the drop in edge pressure.

Consequently, in these H-mode discharges, the edge barrier appears to be responsible for the main part of the confinement loss towards $\delta_{top} < 0$. It is too early to establish the separate role of core and edge transport. In fact, with $\nu_{eff} \sim 1$ in the TCV H-mode at $\delta_{top} = \pm 0.2$, core transport improvement towards $\delta_{top} < 0$ should not be dominant [9, Fig. 6]. In order to take full advantage of the confinement improvement at negative triangularity, the collisionality in H-modes has to be reduced. Since in TCV H-mode the density cannot be lowered further, due to the H-mode low-density limit, a higher temperature with supplementary core electron heating (X3, O2) seems necessary. In a reactor, this low collisionality condition should be favoured by central electron α-heating.

5. H-mode Stability, δ-Scan

This section presents the ideal MHD stability analysis of the above triangularity scan, which has demonstrated a reduction of the ELM energy loss. In addition, possible ways of improving edge stability of negative triangularity plasmas shapes in terms of pressure limits are described, exploring different shapes including X-point(s) or snowflake divertor located on the low field side (LFS).

The KINX code was developed for ideal stability calculations in the presence of an X-point [18]. The effect of a snowflake divertor was analyzed recently [19]. The case of negative triangularity and the influence of the major radius of the X-point were specifically studied in preparation of the experiments presented here [20].

KINX calculations for equilibria with SNC and with increasingly $\delta_{top} < 0$ show that the $n = \infty$ ballooning mode limit moves gradually to smaller pressure gradients, see Fig. 9, closing the access to the 2nd stability region.

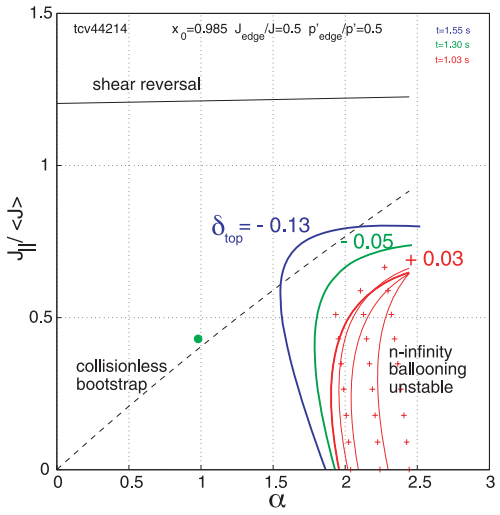

Fig. 9 Triangularity δ_{top}-scan for SNC equilibria (see Fig. 5), showing the shrinking and final disappearance of the accessible 2nd stability domain towards $\delta_{top} < 0$.

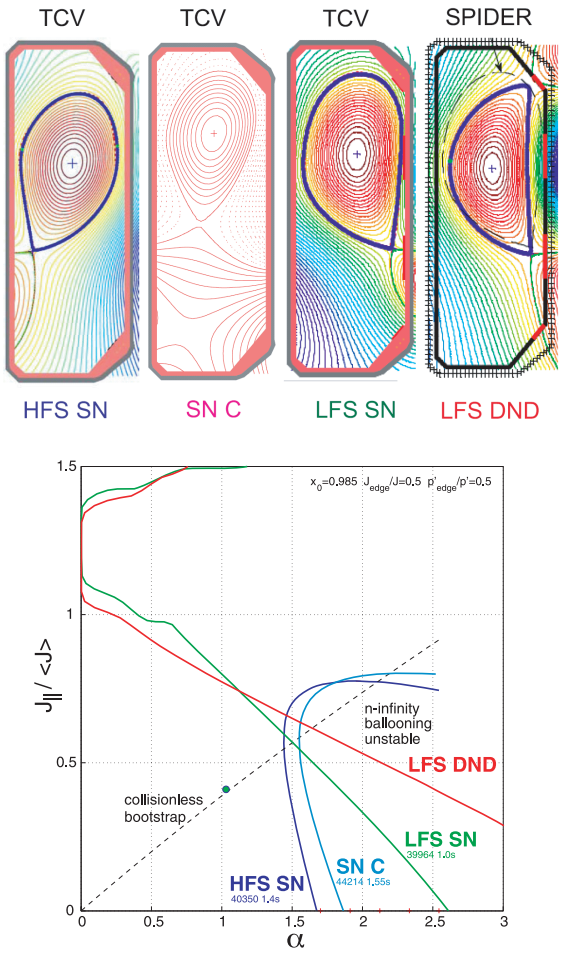

Fig. 10 The displacement of the X-point major radius to larger values, keeping similar negative upper triangularity and elongation, opens progressively the low $J_\parallel/\langle J\rangle$ domain to larger pressure gradients. The collisionless bootstrap values (dotted line) do not change much from equilibrium to equilibrium, so that only one of them, #40350 $t = 1.4$ s (HFS SN) is shown. The pedestal parameters during the shot are expected to be well below the bootstrap line due to the finite collisionality.

Here the stability maps are presented as functions of the normalized parallel current density $J_\parallel/\langle J\rangle$ and normalized pressure gradient α, taken at the position of maximal pressure gradient in the pedestal [19]. The thick lines show the ballooning limit at the maximum of the pressure gradient in the pedestal. Red crosses and thin solid lines show the overall instability region taking into account all magnetic surfaces across the pedestal for $\delta_{top} = +0.03$. The collisionless bootstrap current values (dotted line) do not change significantly from equilibrium to equilibrium (all from shot #44214) so that only one of them is shown ($t = 1.03$ s). The pedestal parameters during the shot are expected to be well below the bootstrap line due to the finite collisionality. The green circle shows the pedestal parameters of the base equilibrium used for the generation of the edge stability diagrams.

This leads to a decrease of the edge pressure gradient and thus of the edge pressure pedestal (Fig. 8), and hence of the ELM amplitude (Fig. 7), both indeed found in the experiment. Note that the $n = \infty$ ballooning mode limit is the first MHD stability limit, which is a typical feature of the edge stability of negative triangularity equilibria [20–22]. More details on beta limits against global kink modes for different plasma profiles at negative triangularity are in [23].

These initial experiments in just one kind of equilibrium class with negative triangularity show already that negative triangularity H-mode with $\delta_{top} < 0$ has the potential to mitigate ELMs and should therefore be further explored for a larger class of configurations.

For example, the effect of moving the X-point towards LFS is explored in a series of equilibria shown in Fig. 10: The two on the left, the high field side single null and the single null centred (HFS SN, SN C) have been operated in H-mode till $\delta_{top} \sim -0.25$ (for HFS SN results, see [24]). The 2nd (SN C) enabled reliable H-mode operation (as described in section 4), the 3rd, the low field side single null (LFS SN) was not yet developed to H-mode, the 4th, the low field side double null (LFS DND) is only artificial. With the X-point moving to the LFS, stability calculations show that a region of "1st stability" at low values of $J_\parallel/\langle J\rangle$ extends to larger α, because of the higher edge shear. Adding a further X-point to produce a double null divertor (DND) configuration reinforces this effect [20]. Since the experimental points in this diagram generally lie somewhat below the collisionless bootstrap line, these schemes enlarging the 1st stability region should be advantageous.

The snowflake divertor concept was tested and developed for the first time in TCV [25] following the proposal by Ryutov [26], and studied in H-mode in TCV [27]. The ELM characteristics changed from X-point to snowflake

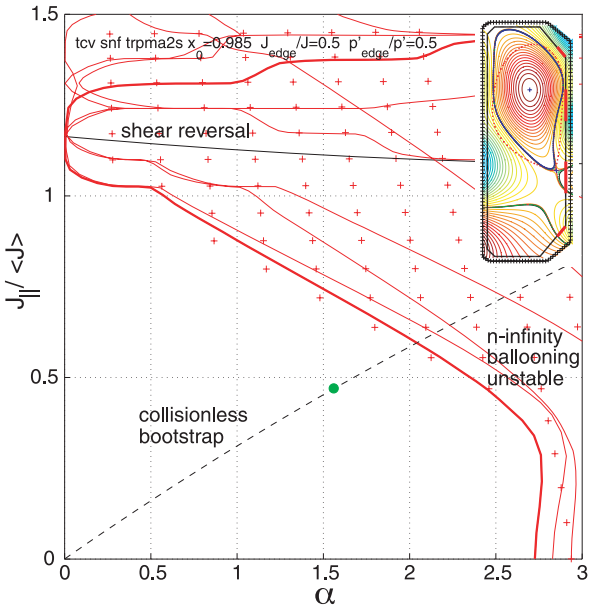

Fig. 11 Snowflake on the LFS further increases the ballooning stable domain to higher $J_{\|}$, (LFS snowflake SF+ equilibrium shown in the insert, $\kappa = 2$, $\delta_{\rm top} = +0.5$, $\delta_{\rm bot} = -0.8$) [20]. The pedestal parameters during the shot are expected to be well below the bootstrap line due to the finite collisionality.

plus SF+ divertor, with a decrease in ELM frequency ($\times \sim 0.3$) and ELM average heat fluxes ($\times \sim 0.4$), although $\Delta W_{\rm ELM}/W$ was found to increase ($\times \sim$1.2-1.3), probably linked to the higher pedestal stability (ideal MHD) [27, Fig. 5c]. Part of the ELM characteristics changes may be due to the inherent, though slight, shape change, as the divertor goes from quadrupole to hexapole null.

Starting from a LFS SN, it is possible to substitute the X-point on the LFS by a snowflake (SF+) divertor, which further improves stability by increasing the edge shear. This further opens 1st stability to high α, and also to higher $J_{\|}/\langle J\rangle$ [20], as shown in Fig. 11. This equilibrium is stable up to $\beta_{\rm N} \sim 3$ for n = 1-3 modes, and is compatible with TCV coil current requirements [20].

In summary, the initial experiments in TCV have demonstrated the potential to mitigate ELM heat losses by applying negative triangularity.

It would be of interest to develop these experiments in the direction of a LFS divertor that advantageously increases the power damping surface and in the direction of a LFS snowflake divertor, which can distribute the conducted power to target plates with 4 instead of 2 divertor legs and has an increased radiation volume due to the 2nd order null, while being more stable.

6. Conclusions and Outlook

The beneficial effect of negative triangularity on energy confinement and radial heat transport was investigated. Although the geometric triangularity vanishes totally at the core, the measurements reveal that the heat diffusivity is reduced by negative triangularity all the way to the core. Similarly, the confinement response to a radial scan of power deposition shows a major increase for $\delta < 0$, even for regions close to plasma axis.

On the modelling side, *local* non-linear gyrokinetic simulations explain the effect of shape on heat diffusivity in terms of resonance tuning between the TEM and the trapped electron precession frequency. However, they are unable to account for the deep radial penetration of the transport modifications. *Global* gyrokinetic simulations in the TEM regime predict that the improvement in the transport, estimated using mixing length arguments results from low-n TEM-modes of large radial extension. This radial extension, which couples core and edge, calls for a *global* transport analysis.

Initial studies of H-mode with negative triangularity in single null centred discharges demonstrate significant mitigation of type I ELM peak power losses with negative triangularity (factor 3 in the range $-0.2 < \delta_{\rm top} < +0.2$). This mitigation is obtained at the expense of a reduction of the pedestal height.

Whether core confinement improvement at negative triangularity can compensate the confinement loss at the pedestal depends on the turbulence regime. From earlier experience, the collisionality in these TCV H-modes in the reactor-relevant TEM-dominated regime appears high to allow for clear core transport triangularity effects to develop.

It would be desirable to extend the study of the two issues of core confinement improvement and ELM mitigation towards negative triangularity on identical equilibria classes in the low collisional domain. A first next step would be to repeat the confinement and transport triangularity dependence study [9] on the SNC equilibria used in section 4. Since the low collisionality regime may be difficult to access in TCV H-mode, complementary studies may be needed in other large devices with electron heating.

It is thought that in order to get the favourable effect of negative triangularity in a reactor, one needs low collisionality TEM regime together with global transport effects persisting at higher ρ^*-values. The proper confinement regimes in the reactor are a matter of debate, although TEM turbulence dominated regime in the presence of central electron α-heating is plausible. Whether these conditions will be fulfilled in a reactor plasma is not known yet, but such issue will soon be within the reach of high-performance computing (HPC) gyrokinetic calculations [28].

Innovative candidate shapes with negative triangularity are proposed for exploration in TCV, including a LFS snowflake, or DND on the LFS, which, by increasing the edge shear, increases substantially the edge pressure gradient in the 1st stability domain.

This work was supported in part by the Swiss National Science Foundation.

[1] A. Pochelon, Y. Camenen, A. Marinoni *et al.*, Proc. of 22nd IAEA Fusion Energy Conference, Geneva, Switzerland, 12-18 Oct 2008, EX/P5-15.
[2] F. Hofmann *et al.*, Plasma Phys. Control. Fusion **36**, B277 (1994).
[3] T.P. Goodman and the TCV Team, Nucl. Fusion **48**, 054011 (2008).
[4] A. Pochelon, T.P. Goodman, M.A. Henderson *et al.*, Nucl. Fusion **39**, 1807 (1999).
[5] A. Pochelon, S. Coda *et al.*, 26th EPS Conf on Plasma Phys., ECA Vol.**23J**, 1089, P3.36 (1999).
[6] J-M. Moret *et al.*, Phys. Rev. Lett. **79**, 2057 (1997).
[7] Y. Camenen *et al.*, Plasma Phys. Control. Fusion **47**, 1971 (2005).
[8] C. Angioni *et al.*, Phys. Plasmas **10**, 3225 (2003).
[9] Y. Camenen *et al.*, Nucl. Fusion **47**, 510 (2007).
[10] A. Marinoni *et al.*, Plasma Phys. Control. Fusion **51**, 055016 (2009).
[11] N. Kirneva *et al.*, Plasma Phys. Control. Fusion **54**, 015011 (2012).
[12] M. Kotschenreuther, G. Rewoldt and W.M. Tang, Comput. Phys. Commun. **88**, 128 (1995).
[13] S. Jolliet *et al.*, Comput. Phys. Commun. **177**, 409 (2007).
[14] S. Jolliet, EPFL Thesis no. 4326 (2009).
[15] J.-M. Moret, F. Buhlmann and G. Tonetti, Rev. Sci. Instrum. **74**, 4634 (2003).
[16] J.X. Rossel, EPFL thesis no. 5311 (2012); J.X. Rossel, J.-M. Moret *et al.*, Nucl. Fusion **52**, 032004 (2012).
[17] J. Stober *et al.*, Plasma Phys. Control. Fusion **42**, A211 (2000).
[18] L. Degtyarev *et al.*, Comput. Phys. Commun. **103**, 10 (1997).
[19] S.Yu. Medvedev *et al.*, Contrib. Plasma Phys. **50**, 324 (2010).
[20] S.Yu. Medvedev *et al.*, 38th EPS Conf on Plasma Phys., P2.093 (2011).
[21] S.Yu. Medvedev, 37th EPS, ECA Vol.**34A** P4.145 (2010).
[22] S.Yu. Medvedev, 36th EPS, ECA Vol.**33E**, P2.143 (2009).
[23] S.Yu. Medvedev, 35th EPS, ECA Vol.**32D**, P1.072 (2008).
[24] A. Pitzschke, EPFL Thesis no. 4917 (2011); A. Pitzschke, Plasma Phys. Control. Fusion **54**, 015007 (2012).
[25] F. Piras *et al.*, Plasma Phys. Control. Fusion **51**, 055009 (2009); F. Piras *et al.*, Plasma Phys. Control. Fusion **52**, 124010 (2010).
[26] D.D. Ryutov *et al.*, Phys. Plasmas **15**, 092501 (2008).
[27] F. Piras *et al.*, Phys. Rev. Lett. **105**, 155003 (2010).
[28] L. Villard *et al.*, Plasma Phys. Control. Fusion **52**, 124038 (2010).